Structural characterization of sodium azide and sodium bifluoride at high pressures

DOI 10.1515/zkri-2013-1660 — Z. Kristallogr. 2014; 229(3): 259–275

David I. A. Millar, Christopher Barry, William G. Marshall and Colin R. Pulham*

Structural characterization of sodium azide and sodium bifluoride at high pressures

Abstract: This paper reports the structural characterization of sodium azide and sodium bifluoride (hydrogenfluoride) at elevated pressures using neutron powder diffraction. Compression of sodium azide at 294 K induces a transition from the β-phase to the α-phase. This structure responds to increasing pressure by progressive tilting of the azide groups. Compression of the α-form to 3.33 GPa at 393 K results in a phase transition to the tetragonal γ-phase (space group $I4/mcm$), which is isostructural with the azides of the heavier Group 1 elements and features square-antiprism co-ordination of the cations. On decompression at ambient temperature, the γ-phase reverts to the α-phase, but with substantial peak broadening indicative of significant strain within the recovered sample. Compression of sodium bifluoride ($NaDF_2$-I to 0.66 GPa at ambient temperature resulted in the formation of $NaDF_2$-II, which adopts an orthorhombic, marcasite-like (space group $Pnnm$) structure. Further compression to 4.58 GPa resulted in a transition to $NaDF_2$-III, which adopts the archetypal $I4/mcm$ structure shared by the heavier alkali metal bifluorides and γ-NaN_3.

Keywords: high pressure, azide, bifluoride, neutron diffraction, crystal structure

*Corresponding Author: Colin R. Pulham, School of Chemistry and Centre for Science at Extreme Conditions, The University of Edinburgh, King's Buildings, West Mains Road, Edinburgh, UK EH9 3JJ. Fax: +44 (0) 131 650 4743;
Phone: +44 (0) 131 650 4756, e-mail: c.r.pulham@ed.ac.uk
David I. A. Millar, Christopher Barry, William G. Marshall: ISIS Neutron and Muon Facility, STFC Rutherford Appleton Laboratory, Harwell Oxford, Didcot, UK OX11 0QX

1 Introduction

Ionic crystals with spherical cations and rod-like anions, for example the azides (N_3^-), bifluorides (HF_2^-) and thiocyanates (SCN^-) of the alkali metals, are of significant interest to both experimental structural scientists and theoreticians. The relative simplicity of their crystal structures at ambient conditions (they are related to either of the NaCl or CsCl prototypical structures) means that experimental results are reasonably straightforward to interpret. Furthermore, these simple systems are prime candidates for theoretical studies examining electronic, vibrational and elastic properties and for modelling high-energy processes, such as explosive decomposition [1–3]. This is especially true for the metal azides, which have been widely used as gas generators on account of their rapid decomposition to produce large amounts of N_2(g). Sodium azide, for example, has been used in automotive air-bags [4].

Despite this structural simplicity at ambient temperature and pressure, these compounds exhibit remarkable polymorphism under non-ambient conditions. Indeed the structural variety displayed by the Group 1 azides, bifluorides and thiocyanates has inspired a prodigious body of work exploring their pressure/temperature phase diagrams using practically every available analytical technique from microscopy to diffraction and from spectroscopy to calorimetry; the majority of this work has been comprehensively reviewed by Fuith [5] and Schranz [6]. Nevertheless, numerous phases that are formed at elevated pressures have yet to be structurally characterized. In this context we present the structure determination of γ-NaN_3, a form obtained at elevated temperatures *and* pressures, and the re-determination of two high-pressure phases of sodium bifluoride obtained by compression (to 0.6 and 4.3 GPa, respectively) at ambient temperature.

Sodium azide, NaN_3

Sodium azide may adopt either of two crystal structures at atmospheric pressure, depending on temperature. The rhombohedral ($R\bar{3}m$) structure of the high-temperature β-form ($T > 292$ K) may be regarded as a distortion of the cubic NaCl structure, in which the chloride anions are replaced by the rod-like azide ions (N_3^-) [7–11]. The azide ions lie parallel to the body diagonal of the former NaCl unit cell and the body diagonal thus becomes elongated. It is also possible to define a monoclinic unit cell for β-NaN_3 that facilitates comparison with the low temperature α-form ($C2/m$), Fig. 1. The structure of α-NaN_3 was

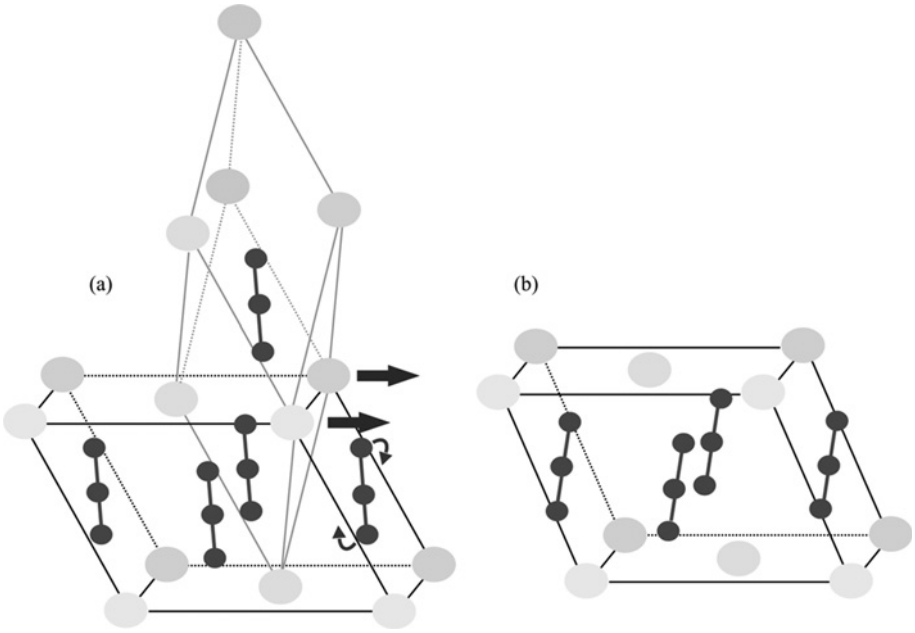

Fig. 1: Comparison of β- and α-NaN_3: (a) in addition to the rhombohedral unit cell, a monoclinic structure may be selected for β-NaN_3. Upon the $\beta \rightarrow \alpha$ transition, the azide anions undergo a slight rotation and the cation layers are sheared. The monoclinic structure of α-NaN_3 is shown in (b).

first determined by X-ray powder diffraction on samples cooled from the β-form [9]. The X-ray powder diffraction patterns led the authors to propose a displacive model for the $\beta \rightarrow \alpha$ transition in which the layers of sodium atoms are sheared perpendicular to the *b*-axis and the azide ions are tilted away from the original body diagonal (see Fig. 1). The structure of the α-form was later confirmed by a combination of X-ray single-crystal and powder diffraction [12].

The $\beta \rightarrow \alpha$ phase transition in sodium azide (observed at a transition temperature, T_c, between 286 and 295 K) [13] has been studied by numerous analytical techniques in order to establish its true nature, i.e. is it weakly first order or a continuous second-order phase transition? The apparent second-order behaviour was initially described using an order-disorder model [9, 14, 15]. It was also observed that degenerate Raman modes split [13, 16], indicating a group-subgroup relationship between the symmetries of the two phases. Choi and Prince proposed a disordered model of the high-temperature phase on the basis of their neutron diffraction experiments [10].

Heat capacity measurements were unfortunately ambiguous: any discontinuities or thermal hysteresis loops were too small for the authors to be confident in excluding experimental error [17, 18]. Furthermore the results were significantly dependent on sample preparation – inhomogeneous strain within the sample gave rise to smearing of the specific heat anomaly, which could be mistaken for a continuous transition [18]. Midorikawa et al., however, were able to observe by polarizing microscopy a distinct phase front between two phase domains in a single crystal of sodium azide [19]. At the same time, Hirotsu's study of the birefringence of a single crystal also gave clear evidence for a first order transition [20]. These contemporaneous results had a significant impact on opinion in the literature – subsequent observations have been contextualised using models that emphasise the displacive nature of the transition [21–24]

Careful measurements of the unit cell parameters and symmetry-breaking shear strains as a function of temperature between 12 and 295 K confirmed that the transition involves a coupling of the canting of the azide anion (order-disorder) with the shearing of the sodium layers (displacive) [12]. This is illustrated in Fig. 1. As a final corroboration the authors reported a small discontinuity in their measurements at 292.2 K that led them to conclude that this was the exact transition temperature, that the phase transition is ferroelastic, and that it is weakly first order.

In addition to the considerable interest in the structural modifications of sodium azide within a few degrees of room temperature, there have been diffraction and spectroscopic studies undertaken at high temperatures and/or high pressure. No phase transitions from the β-form were observed on heating NaN_3 to its decomposition point (548 K) at atmospheric pressure [25]. Increasing pressure at ambient temperature, however, seems to parallel the effect of cooling at ambient pressure. Bradley et al. first observed a splitting in their X-ray powder diffraction patterns upon increasing pressure to 0.25 GPa [26]. Although structure determination was not possible in this case, the authors noted the similarity with the $\beta \rightarrow \alpha$ transition on cooling and proposed that a similar

transition could occur on compression. In their pioneering work on the compressibility of energetic materials, Weir et al. were able to apply the 'new' diamond-anvil cell technology to carry out single-crystal X-ray diffraction studies on NaN_3 [27]. They obtained a monoclinic for unit cell for sodium azide at ~1.0 GPa, which was consistent with the low-temperature α-form.

Comparison of Raman spectra collected for the high-pressure form with those for the low-temperature α-form also confirmed that they were indeed the same phase [24]. Furthermore, it was possible to plot the linear pressure/temperature dependence of the β/α phase line between 0–0.3 GPa and 253–373 K. The pressure range for spectroscopic studies was later extended to 4.0 GPa by Christoe and Iqbal, who noted that the $\beta \rightarrow \alpha$ transition occurs at 0.07 GPa and that, once formed, the α-form remains stable to the highest pressures studied [28]. More recently neutron powder diffraction has been used to observe the structural response of α-NaN_3 to compression (up to a maximum pressure of 1.2 GPa). Rietveld refinement of data collected at 0.5 GPa shows that compression involves both a distortion of the unit cell and a tilt of the linear anions in the monoclinic plane [29]. Very recently, sodium azide has been investigated by *in situ* synchrotron X-ray diffraction measurements in a diamond anvil cell up to 52.0 GPa at room temperature three different pressure transmitting media [30]. Three pressure-induced phase transitions were observed at pressures of 0.3, 17.3, and 28.7 GPa. The transition at 0.3 GPa was characterized as the $\beta \rightarrow \alpha$ transition and an equation of state for the α-phase was reported. On the basis of the diffraction patterns collected for the second high-pressure phase, the authors suggest that this has a lower symmetry than that of the α-phase [30].

The combined effects of elevated temperatures *and* pressures, however, are sufficient to drive sodium azide into another distinct phase, referred to in the literature as both y-NaN_3 and NaN_3-III. A volume discontinuity was observed during compression of the β-form at ~357 K (between 2.6 and 3.0 GPa) [31]. This $\beta \rightarrow y$ transition is reported to be quite sluggish, but proceeded much more quickly when compression was performed at 373 K. It was also possible to observe a transition from the α-form to the y-form at 333 K and 2.8 GPa, but this transition was so sluggish at lower temperatures that it became 'virtually unobservable'.

High-pressure techniques have recently been proposed for the production of polynitrogen species using sodium azide as the precursor. Such species are to be regarded as 'high-energy density materials' that would be expected to burn rapidly with the release of environmentally clean by-products. Peiris et al. have reported evidence for the formation of N_7^- species upon photolysis ($\lambda = 514$ nm) of a polycrystalline sample of NaN_3 at ca. 5.0 GPa [32]. Eremets et al., however, noted that the application of pressure alone was sufficient to create a phase composed of clusters of nitrogen atoms ($P > 19$ GPa) and a disordered non-molecular phase (50–120 GPa), although these phase transitions could be accelerated by the application of shear stress or by laser heating [33].

Before the high-pressure synthesis of polynitrogen species can be explored further, however, we feel it is essential that the behaviour of sodium azide under extreme conditions is fully understood. Principally, this requires the structure solution of y-NaN_3 as well as a critical assessment of the ambient-temperature compression behaviour, which will be of significant interest to theoreticians who seek to develop predictive models of these important materials at high pressures. For these reasons, two neutron powder diffraction studies were performed in this work – the compression of α-NaN_3 to 6.0 GPa and the high-pressure, high-temperature study of the y-form.

Sodium bifluoride, $NaHF_2$

For the alkali metal bifluorides (also referred to as metal hydrogenfluorides or acid fluorides), a wealth of experimental and theoretical analyses exists examining the strong hydrogen bonding within the HF_2^- anion. The H...F bond is amongst the strongest H-bonds known and is of the same order as many covalent bonds [34–36]. Moreover, it is the only hydrogen bond in which the proton is located essentially symmetrically between the two fluoride nuclei [37–42], although it has since been shown that it may adopt an asymmetric configuration in structures that possess sufficient electronic and crystal asymmetry to distort the HF_2^- anion from the ideal symmetric configuration, such as in p-toluidinium bifluoride [43].

Like its azide analogue, sodium bifluoride adopts a rhombohedral ($R\bar{3}m$) crystal structure at ambient temperature and pressure [44–47]. However, unlike NaN_3 it does not undergo any temperature-induced phase transitions at atmospheric pressure and therefore no structural analogue of α-NaN_3 exists for $NaHF_2$ [48, 49]. Furthermore, the high-pressure behaviour of sodium bifluoride has been shown to display very little in common with that of sodium azide. While the $\alpha \rightarrow \beta$ transition in NaN_3 was observed at 0.25 GPa by Bradley et al., compression of $NaHF_2$ (in the same study) resulted in a phase transition to a reported orthorhombic phase at 0.85 GPa [26]. However, subsequent examination of the high-pressure

polymorphism suggested not only that this transition pressure was erroneously high (a volume discontinuity was observed at 0.39 GPa), but also that the proposed orthorhombic unit cell for $NaHF_2$-II would result in an unacceptably large volume contraction [31]. In fact, on the basis of their volumetric measurements Pistorius and Campbell-White state that it is 'reasonable to assume that $NaHF_2$-II and NaN_3-III (*sic*) are isostructural... (and) cannot have the tetragonal KN_3 structure'.

The assertion that $NaHF_2$-II does not adopt the *I*4/*mcm* structure of the larger alkali metal bifluorides was supported by comparison of the IR spectra obtained for this phase with those for KHF_2 [50]. Furthermore, significant changes in the vibrational spectra obtained during compression to ca. 4.0 GPa suggested a further high-pressure phase transition occurs at this pressure. The authors of this study noted that the IR spectrum of this new phase, $NaHF_2$-III, is unlike that of KHF_2 but cautioned that the spectrum obtained may be complicated by the presence of some residual $NaHF_2$-II.

Most recently, the high-pressure behaviour (to a maximum pressure of 9.5 GPa) of $NaHF_2$ has been investigated by Raman spectroscopy and energy-dispersive X-ray diffraction [51]. The splitting of the symmetric F–H–F stretching band into two bands was indicative of a phase transition to a structure with $Z' \geq 2$ at 0.5 GPa. The authors also reported changes in the Raman spectra at ca. 4.1 GPa that substantiate the presence of a II/III transition in this pressure regime. Despite considerable overlap in the pressure domains of the three phases, the authors proposed a unit cell for $NaHF_2$ that bore no resemblance to that put forward by Bradley et al. [26], although they noted that it is consistent with the previously observed X-ray diffraction intensities. Instead, Christy et al. proposed a monoclinic (*P*2/*m*) structure for $NaHF_2$, despite this implying a volume contraction almost twice that calculated by Pistorius [31] – In this respect, the authors reasoned that the start and end points of this sluggish transition were not determined sufficiently accurately in the former study. Furthermore, the relatively few diffraction peaks that were observed for $NaHF_2$-III were indexed to a tetragonal unit cell that is related to the ideal *I*4/*mcm* structure of KHF_2. However, the presence of 'superlattice peaks' implied a doubling of the unit cell and instead they proposed a space group of *P*4/*ncc*. Furthermore, they suggested that the bifluoride anions undergo rotations about the *c*-axis *and* out of the *ab*-plane, resulting in an almost eclipsed arrangement (when viewed down the *c*-axis, see Fig. 2).

We have concerns about some of the conclusions drawn by Christy et al. [51], since they used Nujol as a quasi-hydrostatic pressure-transmitting medium. Paraffin oils such as Nujol have a hydrostatic limit of less than 1.0 GPa [52], so the samples are likely to have been under significant deviatoric stress. This has important implications since the inhomogeneous strain in the sample under these conditions may result in phase transitions being suppressed (or promoted) and anisotropic distortion of the unit cell. The observation that $NaHF_2$-I persisted upon compression to 1.8 GPa, over 1.0 GPa beyond the transition pressure reported by previous studies, suggests that the effects of non-hydrostaticity in this case are significant. We believe that this warrants a closer examination under more hydrostatic conditions, in order to

Element	*x*	*y*	*z*
Na	3/4	3/4	1/4
Na	3/4	1/4	1/4
H	0	1/2	0
F	1/8	0.560	-0.100

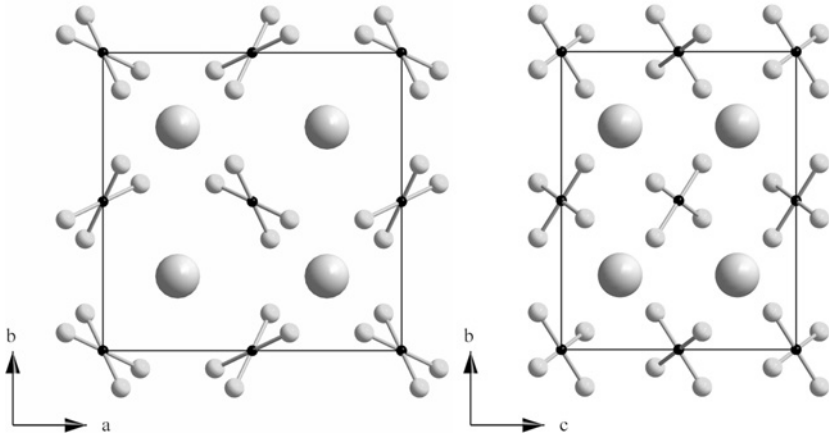

Fig. 2: Representation of the unit cell of NaHF2-II reported by Christy et al. The approximated atomic co-ordinates have also been tabulated for clarity with respect to the origin chosen at ($^1/_4$ $-^1/_4$0).

re-determine the structure of $NaHF_2$-II *and* the I/II transition pressure.

Furthermore we believe that the structure determination of $NaHF_2$-III requires re-examination, since the rationale for the selection of the space group *P*4/*ncc* is perhaps open to question on account of the low resolution energy-dispersive X-ray diffraction data. More importantly though, we believe that the structure suggested by Christy et al. results in an unlikely configuration of the ions. Although this arrangement results in strong Na ... F interactions (ca. 1.99 Å), the repulsive F ... F interactions also shorten dramatically. In the light of this analysis, we reasoned that the high-pressure behaviour of sodium bifluoride merited further study using neutron powder diffraction (under more hydrostatic conditions). Compression of $NaDF_2$ was therefore performed, using perdeuterated methanol : ethanol (in a 4 : 1 ratio) as the pressure-transmitting medium [52] to a maximum pressure of 7.35 GPa.

Experimental

Materials

Polycrystalline samples of NaN_3 (99.5%) were purchased from Sigma-Aldrich and used as received. Sodium fluoride (99.9%, Fischer Scientific) was dissolved in hot aqueous hydrofluoric acid. Sodium bifluoride ($NaHF_2$) crystallized upon cooling, which was then recrystallized from D_2O to produce the deuterated polycrystalline sample ($NaDF_2$) suitable for neutron diffraction studies.

High-pressure neutron powder diffraction

High-pressure neutron powder diffraction data were collected using the PEARL diffractometer at the UK spallation neutron source, ISIS, at the STFC Rutherford Appleton Laboratory. Polycrystalline samples of each compound under investigation (NaN_3 and $NaDF_2$) were loaded, in turn, into a standard profile null-scattering Ti–Zr alloy capsule gasket [53] with perdeuterated methanol : ethanol (4 : 1) as pressure-transmitting medium and Pb as pressure calibrant [54]. The capsule assembly was then compressed with a type V3b Paris-Edinburgh (P-E) press equipped with standard single toroid anvils with cemented WC/Ni binder cores [55]. The P-E press ram pressure was monitored and varied by means of a computer-controlled hydraulic system.

Time-of-flight (ToF) neutron powder diffraction data were collected using the $2\theta = 90°$ detectors with a transverse (through-anvil) scattering geometry. The resulting summed pattern was then normalised with respect to the incident beam monitor and the scattering from a standard vanadium calibration sample. Lastly, the diffraction pattern intensity scale was corrected for the wavelength and scattering-angle dependence of the neutron attenuation by the anvil (WC) and gasket (TiZr) materials. Full-profile Rietveld refinements of the ToF neutron powder diffraction patterns were carried out using the GSAS package [56].

High-pressure/high-temperature neutron powder diffraction

In addition to the ambient-temperature compression experiment described above, NaN_3 was investigated at high pressure *and* high temperature at the PEARL/HiPr beamline (ISIS). In this case, a Paris-Edinburgh V4 cell was equipped with a variable temperature insert to allow rapid heating and cooling *in situ* [57]. Perdeuterated methanol : ethanol (4 : 1) was used as the pressure-transmitting medium and pressures were calibrated to an internal Pb standard. Data were collected and processed using the procedure outlined above.

Results

Sodium azide

High-pressure, ambient-temperature neutron diffraction study

Owing to the low temperature (290 K) in the experimental hutch, the sample, which may have been in the β-form when loaded, gave a diffraction pattern corresponding to the α-form even at ambient pressure. It was possible to refine all of the diffraction patterns collected up to the maximum pressure studied (6.06 GPa) using the α-form, indicating that α-NaN_3 does not undergo a phase transition in this pressure and temperature regime. A multiplot of all of the diffraction patterns collected during compression is shown in Fig. 3, while the unit-cell parameters for α-NaN_3 at each pressure are tabulated in Table 1 and plotted in Fig. 4.

The relative compression of the unit cell axes highlights that the *b*-axis is significantly less compressible than either of the other two, which is consistent with previous compressibility measurements [27]. The greater

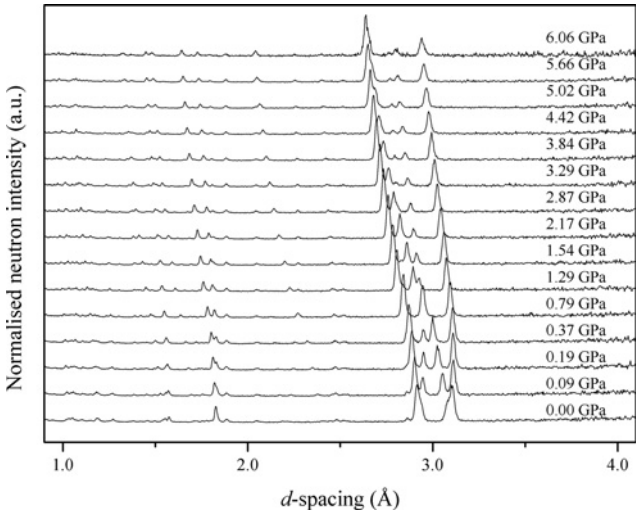

Fig. 3: Multiplot of the neutron powder diffraction patterns collected for α-NaN_3 during compression to a maximum of 6.06 GPa. Other than the gradual movement of peaks to lower *d*-spacing with pressure, no changes indicative of a phase transition are observed.

compressibility of the *a*-axis is perhaps to be expected – this is the direction perpendicular to layers made up of alternating Na^+ and N_3^- ions (see Fig. 5). In the case of the *c*-axis, however, its contraction is accompanied by the large reduction in the β-angle (from 111.5° to 100.8° over 6.0 GPa) as previously reported [30]. Examination of the crystal structure allows one to rationalise the concerted contraction of the *c*-axis and the monoclinic angle in terms of a rotation of the azide ions within the *ac*-plane. Comparison of the structure determined at 5.66 GPa with the ambient-pressure structure (during the same experiment) shows that the azide ion is becoming more oblique to the *c*-axis, allowing the Na^+ cations to pack more closely (see Fig. 5). This compression mechanism is in agreement with that observed by Knorr and Depmeier over a much narrower pressure range (to 1.2 GPa) [29] and by Zhu et al. up to 11.0 GPa [30].

Moreover, the rotation of the azide within the monoclinic plane can be represented graphically by plotting the variation in the angles created between the linear anion and the unit cell *a*- and *c*-axes throughout the compression. Figure 6 shows that this rotation does not display a linear dependence on pressure, but seems to approach a limit at the maximum pressure studied (6.06 GPa). An interesting aspect of the compression of the *b*-axis is that it initially undergoes a small, but significant, expansion before undergoing an almost linear contraction with pressure. The exact reason for this is still unclear, although it is likely that the rotation of the anions may result from or result in this small pressure-induced expansion.

Finally, a 3rd-order Birch-Murnaghan equation of state [58] has been fitted to the isothermal compression of the unit cell volume over the pressure range 0–6.06 GPa. Using Angel's program EoSFIT [59], final values of the refined parameters were: $V_0 = 116.9(2)$ Å^3, $B_0 = 15.1(7)$ GPa and $B' = 7.0(5)$. The unit-cell volume at zero pressure (V_0) is in excellent agreement with the value obtained experimentally [116.75(1) Å^3] determined at atmospheric pressure. These values also agree well with those obtained by Zhu et al., obtained using several pressure-transmitting media [30]. The values of B_0 and B' calculated for α-NaN_3 show that it has very similar compressibility to the isostructural LiN_3 ($B_0 = 19.1(14)$ GPa and $B' = 7.3(5)$) [60] and is comparable, but slightly more compressible, than the alkali halides [61, 62].

Tab. 1: Variation in the unit cell parameters of α-NaN_3 with pressure.

P (GPa)	*a* (Å)	*b* (Å)	*c* (Å)	*β* (°)	*V* (Å^3)	wR_p
0.00	6.3027(4)	3.6526(2)	5.4525(8)	111.551(9)	116.75(1)	0.048
0.09	6.2785(4)	3.6552(2)	5.4070(7)	110.458(8)	116.26(1)	0.059
0.19	6.2483(4)	3.6529(2)	5.3654(7)	109.490(8)	115.45(1)	0.059
0.37	6.2169(3)	3.6478(2)	5.3284(6)	108.687(7)	114.47(1)	0.056
0.79	6.1476(4)	3.6305(2)	5.2588(6)	107.212(9)	112.11(1)	0.055
1.29	6.0720(4)	3.6069(2)	5.1935(6)	105.860(7)	109.41(1)	0.072
1.54	6.0228(4)	3.5901(2)	5.1570(5)	105.086(7)	107.66(1)	0.058
2.17	5.9664(4)	3.5689(2)	5.1160(5)	104.237(7)	105.59(1)	0.061
2.87	5.9122(4)	3.5474(2)	5.0802(5)	103.494(7)	103.61(1)	0.065
3.29	5.8687(4)	3.5298(2)	5.0536(6)	102.909(7)	102.04(1)	0.072
3.84	5.8259(4)	3.5111(2)	5.0280(6)	102.376(8)	100.46(1)	0.073
4.42	5.7879(5)	3.4931(2)	5.0061(6)	101.931(8)	99.03(1)	0.075
5.02	5.7510(5)	3.4766(2)	4.9859(7)	101.506(9)	97.68(1)	0.090
5.66	5.7175(6)	3.4606(2)	4.9685(7)	101.128(10)	96.46(1)	0.084
6.06	5.6924(12)	3.4474(5)	4.9552(14)	100.836(20)	95.51(3)	0.252

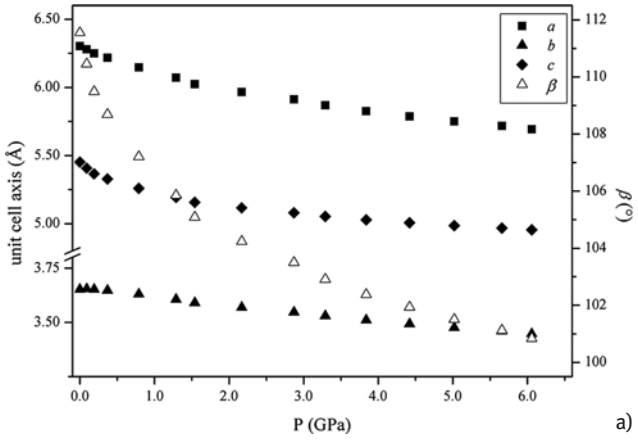

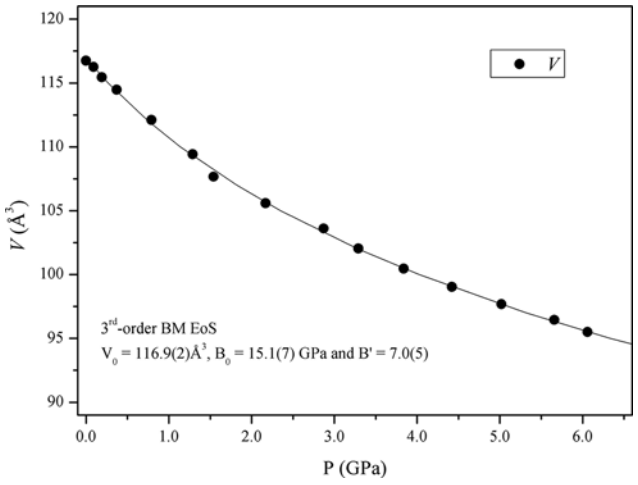

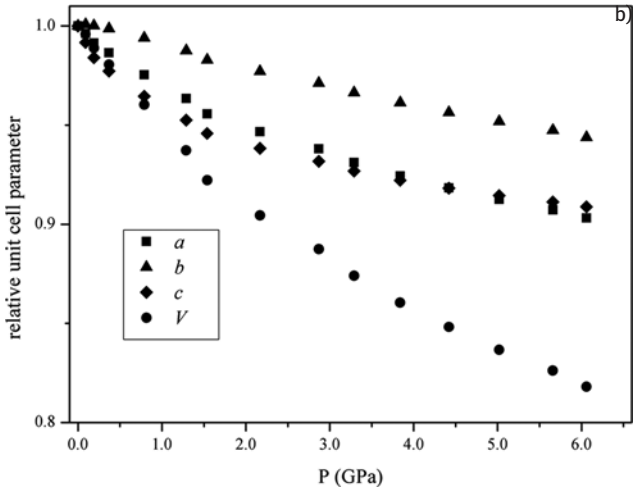

Fig. 4: (a) Compression of the unit cell parameters (a, b, c, and β) of α-NaN_3; (b) smooth variation of unit cell volume, V, with pressure, including 3rd-order Birch-Murnaghan EoS; and, (c) relative compression of the unit cell parameters.

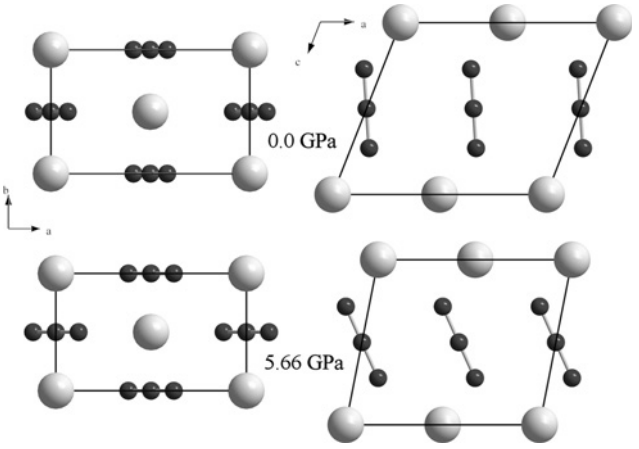

Fig. 5: Comparison of the structures determined at 0.0 GPa and 5.66 GPa: viewed down the c-axis to highlight the interplanar contraction of the a-axis; and viewed down the b-axis to show the rotation of the azide anions in the monoclinic plane.

High-pressure, high-temperature study

In addition to characterizing the high-pressure behaviour of NaN_3 at ambient temperature, the previous observation of a third form of sodium azide at elevated temperatures and pressures motivated further study. As in the previous study, a sample of β-NaN_3 was loaded into the sample capsule in the Paris-Edinburgh press, but this time it was possible to characterize the pressure-induced $\beta \rightarrow \alpha$ phase transition by performing the initial compression at 294 K. The β-form had transformed to the monoclinic α-form by 0.70 GPa. The α-form was then compressed (at 294 K) to 1.91 GPa before warming and pressurising alternately (see Fig. 7) in order to reach the pressure-temperature regime in which Pistorius observed

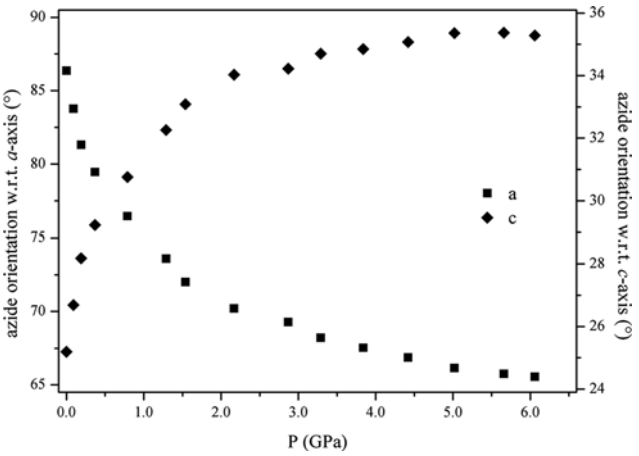

Fig. 6: Azide-ion orientation with respect to the a- and c-axes upon compression.

the *y*-form (2.8 GPa at 333 K) [31]. In accordance with the reported sluggishness of this transition, no changes in the diffraction pattern were observed during this data collection (~0.5 hr).

As the rate of the $\alpha \rightarrow y$ transition was reported to increase at higher temperatures, the sample was slowly warmed to 393 K at constant load, but still no changes in the diffraction patterns were evident over the course of 6 hours. Pattern refinements revealed that the act of heating the sample resulted in an increase in sample pressure from 2.77 GPa to 3.20 GPa, caused by the temperature-induced expansion of the pressure-transmitting medium. If the equilibrium α–y transformation line has a positive slope, increasing pressure should promote the transformation to the *y*-form, but increasing temperature should retard this transformation (the *y*-form is a low-temperature form relative to the α-form).

Increasing the applied load to 40 tns at 393 K (sample pressure 3.22 GPa) resulted in the appearance of weak peaks (~2.32 and ~2.42 Å), which could not be attributed to the α-form. It was only upon further compression to 3.33 GPa, however, that a pure sample of the *y*-form was observed, highlighting the significant kinetic barrier to this transition. The quality of the diffraction pattern collected at 3.33 GPa/393 K was such that it was possible to determine the space group as *I*4/*mcm* [63]. This is the same space group adopted by the azides of the larger alkali metals and full-profile Rietveld refinement was possible using atomic co-ordinates based on the tetragonal structure of CsN_3-II [64]. The quality of the Rietveld refinement for the *y*-form is shown in Fig. 8.

In the tetragonal structure of *y*-NaN_3, the azide anions and sodium cations are organised into alternating layers perpendicular to the *c*-axis. Within the layers, the azide ions are oriented normal to their nearest neighbours, resulting in the favourable interaction between the electronegative termini and electropositive central N-atom. This geometry gives rise to the square-antiprism co-ordination environment, formed by the terminal N-atoms of eight azide anions round one Na^+, rather than the very-slightly-distorted octahedral environment observed in the monoclinic form. The most significant change over the $\alpha \rightarrow y$ transition, however, is in the distances separating neighbouring cation layers. In α-NaN_3 at 3.22 GPa, each cation is surrounded by six others within the same

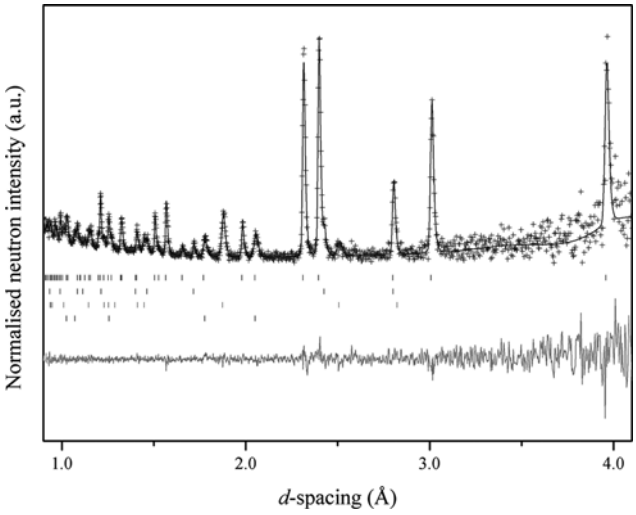

Fig. 8: Rietveld refinement of the pattern collected for *y*-NaN_3 at 3.33 GPa and 393 K. The experimental data (I_{obs}) are represented as crosses, the calculated pattern (I_{calc}) is shown as a solid line, and the difference ($I_{obs} - I_{calc}$) is shown as the lower line. Tick-marks for each phase (*y*-NaN_3, Pb, WC, and Ni) are also shown.

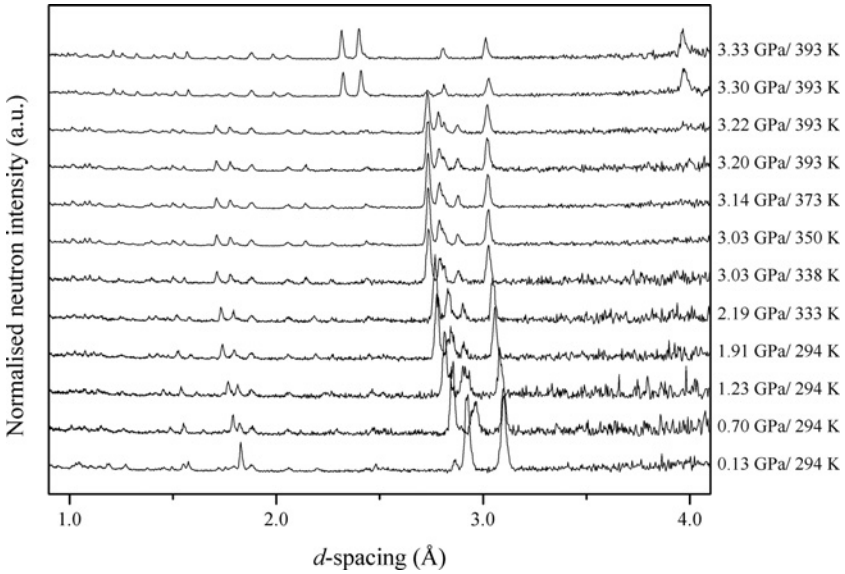

Fig. 7: Neutron powder diffraction patterns collected during the compression/warming of NaN_3 to 3.33 GPa and 393 K. This multiplot shows not only the phase transition from the α-form to the *y*-form, but also the $\beta \rightarrow \alpha$ transition occurring between 0.13 GPa and 0.70 GPa at 294 K.

plane (at distances of either 3.54 or 3.44 Å) and an additional two positioned directly above and below in the neighbouring layers (5.07 Å). In the tetragonal *y*-form at 3.30 GPa the (slight) lengthening of the intraplanar distances between neighbouring cations (to 3.60 Å) is accompanied by a dramatic decrease in the interplanar separation (to 3.01 Å). This is highlighted in Fig. 9. It is this dramatic shortening of the distance between the planes that results in the 7.8% contraction of the molecular volume over the transition (between 3.22 and 3.30 GPa).

Our measurements on the *y*-phase were limited to a pressure of 3.33 GPa and so it is not possible to determine whether this is the same phase identified by Zhu et al. on compression at ambient temperature at 17.3 GPa, and which the authors also denoted as *y*-NaN_3 [30]. On the one hand, it could be that with sufficient pressure alone the *y*-phase can be obtained. However, based on the complexity of the diffraction pattern obtained at 17.3 GPa, the authors suggest a lower symmetry structure compared to the *α*-phase, which would of course not be compatible with the *I*4/*mcm* structure discovered in the current study. Furthermore, it was not possible to fit the peak positions in the pattern obtained at 17.3 GPa with the tetragonal unit cell obtained in the current study.

The significant amount of rearrangement in the structure (and the resultant dramatic reduction in molecular volume) explains the sluggish nature of the transition. Furthermore it suggests that the *y*-form may display significant hysteresis upon cooling and subsequent decompression and may therefore be recoverable to ambient conditions. It was for this reason that we carefully monitored the cooling of *y*-NaN_3 to ambient temperature (at constant load of 51 tns) as well as its decompression, in order to determine the conditions under which it may undergo a phase transition, most likely to the *α*-form.

Cooling from 393 K to 313 K (sample pressure decreased from 3.51 to 3.27 GPa) did not result in any phase transition – the unit cell parameters are tabulated below (Table 2) – and so allows direct comparison between the *α*-form obtained in the ambient temperature compression study above and the *y*-form in the present study. The molecular volume of the *α*-form at 3.29 GPa (293 K) is 102.909(7) $Å^3$, compared to 93.889(17) $Å^3$ obtained for the *y*-form at 3.27 GPa (313 K). This clearly shows that the *y*-form is the denser form (by 8.8%).

It was only upon decompression that the first indications of a phase transition were observed – the pattern collected at 2.47 GPa (300 K) was successfully refined as a mixture of the *α*- and *y*-forms. This suggests that the maximum positive slope for the *α*–*y* transformation line is $\sim 9.25 \times 10^{-3}$ GPa K^{-1}. If extrapolated to 290 K, then the equilibrium pressure for the $\alpha \rightarrow y$ transition should be ~2.38 GPa. Hence the persistence of the *α*-form to 6.06 GPa in this study and to 17.3 GPa in the study by Zhu et al. [30] highlights the remarkable degree of metastability exhibited by the *α*-form at ambient temperature.

Further decompression to 1.32 GPa resulted in a clean pattern of the *α*-form, which remained upon decompression to atmospheric pressure. These patterns, however, showed significant peak broadening when

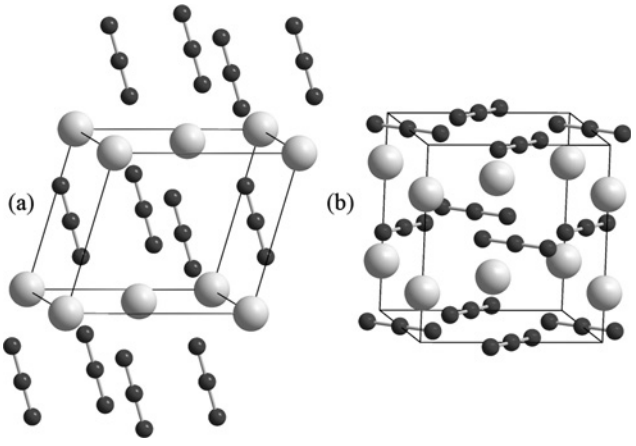

Fig. 9: Comparison of the structures at 393 K of (a) *α*-NaN_3 at 3.22 GPa, and (b) *γ*-NaN_3 at 3.30 GPa. The structures have been oriented such that the rotation of all of the azide anions over the phase transition is highlighted.

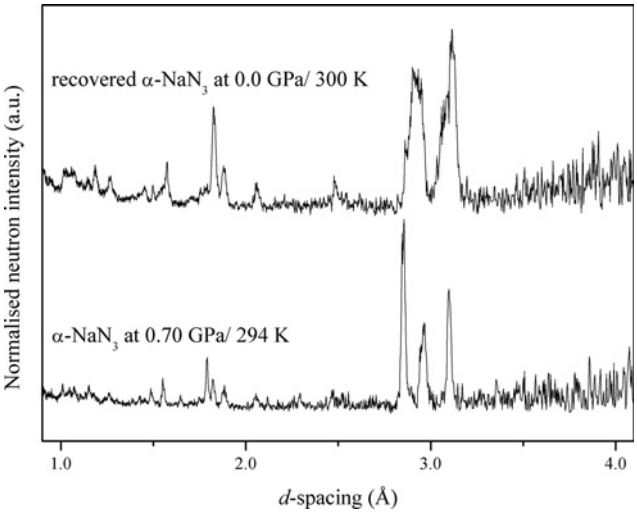

Fig. 10: Comparison of the neutron powder diffraction patterns collected for *α*-NaN_3 before the high-pressure/high-temperature phase transition to the *γ*-form (bottom) and after decompression and cooling (top). The peak broadening in the recovered pattern is clear evidence of significant strain within the sample following the $\gamma \rightarrow \alpha$ transition.

Tab. 2: Unit cell parameters obtained for NaN_3 throughout the variable temperature and pressure neutron powder diffraction study. The pattern collected at 300 K and 2.47 GPa was successfully refined as a mixed phase of both the α- and γ-forms; structural data for both forms is presented under these conditions in the unit cell parameters of α-NaN_3 with pressure.

T (K)	P (GPa)	Form	a (Å)	b (Å)	c (Å)	β (°)	V (Å^3)	wR_p
294	0.13	β	3.64684(17)		15.222(3)		175.32(3)	0.106
294	0.70	α	6.1721(11)	3.6373(6)	5.2817(19)	107.66(3)	113.00(4)	0.199
294	1.23	α	6.0907(12)	3.6139(6)	5.2061(18)	106.11(2)	110.10(4)	0.314
294	1.91	α	6.0055(10)	3.5826(5)	5.1422(14)	104.82(2)	106.96(3)	0.174
333	2.19	α	5.9838(11)	3.5749(5)	5.1316(15)	104.57(2)	106.24(3)	0.211
333	2.46	α	5.9224(10)	3.5493(5)	5.0836(14)	103.64(2)	103.85(3)	0.202
338	3.03	α	5.9139(9)	3.5476(5)	5.0841(14)	103.59(2)	103.68(3)	0.199
350	3.03	α	5.9118(5)	3.5459(2)	5.0802(7)	103.55(1)	103.53(1)	0.063
373	3.14	α	5.9091(5)	3.5439(2)	5.0802(7)	103.53(1)	103.41(1)	0.066
393	3.20	α	5.9073(7)	3.5430(3)	5.0802(10)	103.53(1)	103.37(2)	0.130
393	3.22	α	5.9019(6)	3.5414(3)	5.0732(9)	104.45(1)	103.12(2)	0.083
393	3.30	γ	5.6114(3)		6.0418(4)		190.24(2)	0.082
393	3.33	γ	5.5965(3)		6.0136(4)		188.35(2)	0.082
383	3.47	γ	5.5962(4)		6.0092(6)		188.20(3)	0.195
373	3.34	γ	5.5957(4)		6.0093(5)		188.17(3)	0.146
363	3.35	γ	5.5950(3)		6.0096(4)		188.13(2)	0.089
353	3.24	γ	5.5947(4)		6.0076(5)		188.04(2)	0.205
343	3.29	γ	5.5943(3)		6.0063(5)		187.97(2)	0.149
333	3.28	γ	5.5937(3)		6.0047(4)		187.88(2)	0.077
313	3.27	γ	5.5932(3)		6.0023(4)		187.78(2)	0.078
300	2.47	γ	5.6169(4)	3.5512(2)	6.0553(6)	103.96(7)	191.04(3)	0.116
		α	5.933(3)		5.079(5)		103.85(9)	
300	1.32	α	6.068(2)	3.6006(9)	5.187(3)	105.85(4)	109.02(6)	0.207
300	0.00	α	6.2957(14)	3.6573(8)	5.434(2)	110.70(3)	117.04(5)	0.134

compared to the lowest pressure pattern obtained for the *same* form during compression (shown in Fig. 10). Although the shorter data collection time for the recovered form has certainly resulted in a lower signal-to-noise ratio, this would be not be expected to have an effect on the observed peak-widths. Peak broadening in this case is therefore indicative of significant strain within the sample, arising from the considerable re-arrangement required during the $\gamma \rightarrow \alpha$ transition.

Sodium bifluoride

By applying load to the Paris-Edinburgh cell in very small increments, it was possible to obtain high-quality diffraction data on the rhombohedral form up to a maximum pressure of 0.51 GPa, as shown in Fig. 11 and Table 3. Full-profile Rietveld refinement of the neutron powder diffraction patterns collected for this phase demonstrated that form I undergoes a rather surprising compression mechanism. Rather than compression being manifested in a reduction of the long axis (in fact, within the limits of statistical significance the c-axis does not shorten), it is the ab-plane that undergoes the most significant contraction. While it is difficult to rationalise this marked anisotropy, this observation is in accordance with previous compression studies [51]. It is clear that the shortening of the a-axis results in a strengthening of the interactions between each cation and the fluorine termini of its six nearest neighbouring anions (arranged in a trigonal prism). Along the c-axis, however, as noted by Christy et al. the anions may act as rigid braces [51] – we do not observe any significant shortening of the D-F distances within the anion, nor is there any evidence to sug-

Tab. 3. Summary of the unit cell data obtained during compression of $NaDF_2$-I. In order to facilitate comparison with the higher-pressure forms, the molecular volume (V_{mol}) has also been presented.

P (GPa)	a (Å)	c (Å)	V (Å^3)	V_{mol} (Å^3)	wR_p
0.00	3.4696(2)	13.749(3)	143.34(3)	47.78(3)	0.079
0.01	3.4642(3)	13.750(5)	142.90(5)	47.63(5)	0.173
0.30	3.4483(2)	13.737(4)	141.46(4)	47.15(4)	0.104
0.45	3.4387(2)	13.726(4)	140.56(4)	46.85(4)	0.114
0.51	3.4340(5)	13.739(9)	140.31(9)	46.77(9)	0.125

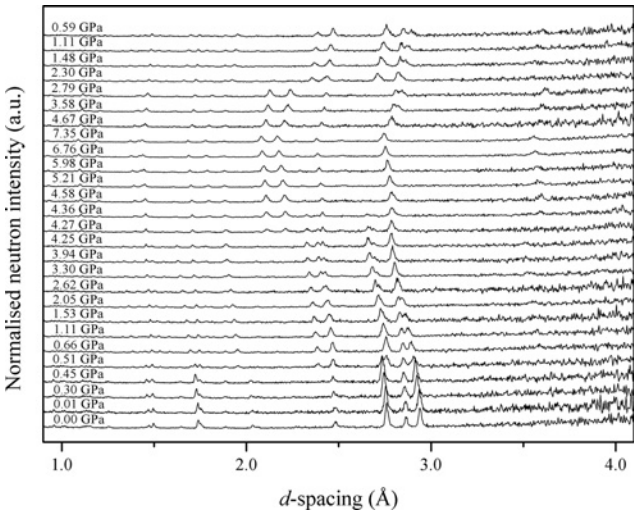

Fig. 11: Neutron powder diffraction patterns collected during the compression (and decompression) of $NaDF_2$.

gest a reduction in space group symmetry indicative of a rotation of the bifluoride ions away from the *c*-axis, as shown in Fig. 12.

At the next pressure point (0.66 GPa), however, a significant change in the neutron powder diffraction pattern was observed, indicative of a phase transition to $NaDF_2$-II. This transition pressure (i.e. between 0.51 and 0.66 GPa) is intermediate to those reported by Bradley et al. [26] and Pistorius [31], but is in close agreement with the spectroscopic analysis of Christy et al. [51]. However, it is important to note that we do not observe any diffraction peaks attributable to $NaDF_2$-I above this transition pressure. Since the pressure-transmitting medium used in this study (4 : 1 MeOD : EtOD) ensured that hydrostaticity was maintained throughout, one may conclude that the reported persistence of this form to 1.8 GPa was directly related to inhomogeneous stresses and strains within the sample resulting from the selection of Nujol as a 'quasihydrostatic pressure medium'.

Furthermore, it has been possible to perform full-profile Rietveld refinements on the diffraction patterns collected for this form using an orthorhombic marcasite-like (*Pnnm*) structure [65], which is closely related to the monoclinic form (*P*2/*m*) suggested by Christy et al. [51].

Tab. 4. Fractional atomic coordinates for the three phases of $NaDF_2$

Phase		*x*	*y*	*z*
$NaDF_2$-I at 0.0 GPa	Na	0.0	0.0	0.0
	F	0.0	0.0	0.4170(5)
	D	0.0	0.0	0.5
$NaDF_2$-II at 0.66 GPa	Na	0.0	0.0	0.0
	F	0.1948(13)	0.3819(10)	0.0
	D	0.0	0.5	0.0
$NaDF_2$-III at 4.58 GPa	Na	0.5	0.5	0.75
	F	0.8406(10)	0.6594(10)	0.5
	D	0.0	0.5	0.5

As shown in Fig. 13, the entire diffraction profile in the present study may be suitably modelled using the *Pnnm* structure and, in fact, the introduction of a monoclinic distortion introduces significant intensity mismatches throughout the pattern. Table 4 gives the fractional coordinates for $NaDF_2$-I and $NaDF_2$-II.

Comparison of the *Pnnm* structure adopted at 0.66 GPa with that of $NaDF_2$-I (see Fig. 14) highlights the dramatic rearrangement that must occur over this phase transition. While the rhombohedral form I may be best described as a layered structure with alternating layers of cations and anions, in form II these layers have become interlocked. This results in a considerable shortening of the cation separation (from 4.990(3) Å to 4.000(5) Å) and a rotation of the anions so that they lie at 45° to the orthorhombic *c*-axis. It is also evident that in the orthorhombic phase there now arises a differentiation between two sets of Na ... F interactions: intraplanar interactions (2.313(4) Å) between each cation and its four nearest neighbouring anions; and, interplanar interactions (2.297(6) Å) with a further two bifluoride ions. Consequently, one observes a change in the sodium co-ordination environment from a trigonal prism in the rhombohedral form to a distorted octahedron in $NaHF_2$-II. It is therefore not surprising that the phase transition is first order, with a volume decrease of ca. 6% – this is in good agreement with the volumetric data reported by Pistorius [31].

It is interesting to note that there is very little change in the co-ordination environment of the bifluoride anions over the transition. Moreover, there is no increase in the

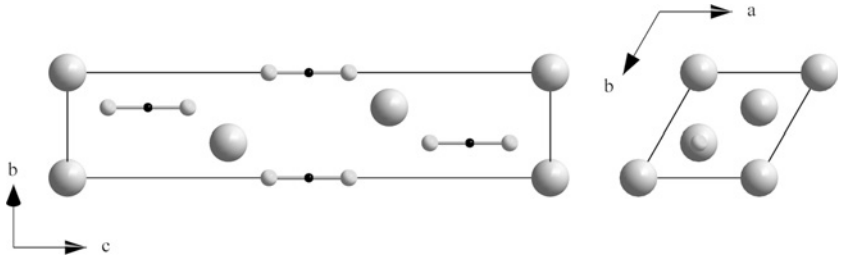

Fig. 12: The rhombohedral structure of $NaDF_2$-I as determined at 0.51 GPa showing the alignment of the bifluoride ions with the *c*-axis.

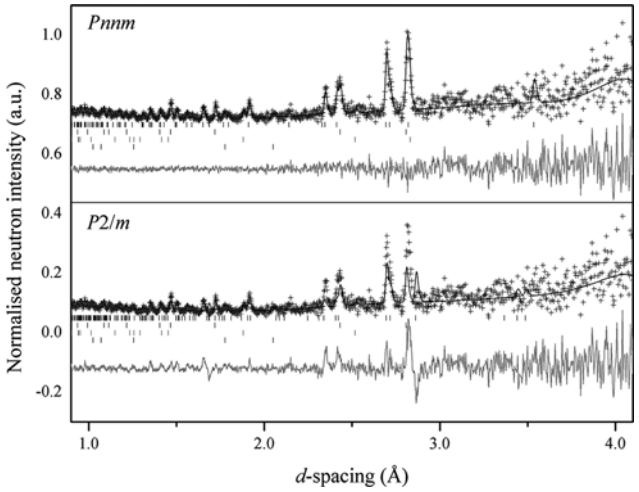

Fig. 13: Comparison of the Rietveld refinements of the pattern collected at 2.62 GPa using the *Pnnm* and *P*2/*m* structural models. The experimental data (I_{obs}) are represented as crosses, the calculated pattern (I_{calc}) is shown as a solid line, and the difference ($I_{obs} - I_{calc}$) is shown as the lower line. Tick-marks for each phase ($NaDF_2$-II, Pb, WC, and Ni) are also shown.

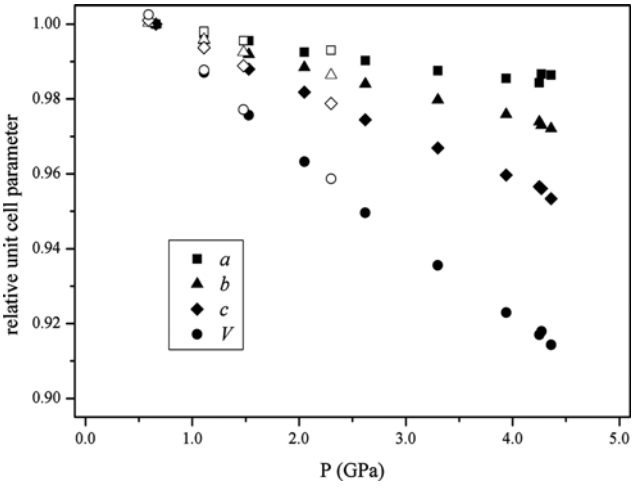

Fig. 15: Relative compression of the unit cell parameters (*a*, *b*, *c*, *V*) of $NaDF_2$-II. It should be noted that the data points collected at 4.27 and 4.36 GPa were derived from a mixed phase and the standard errors of these are larger (*ca* 0.1%). Changes in the relative compression of the unit cell axes at these pressures, therefore, is not believed to be significant. In addition to the data obtained during compression, those collected during decompression of $NaDF_2$-II are presented; these are shown as open symbols.

number of anions in the asymmetric unit. Therefore we cannot reconcile the current structural model with the spectroscopic observations of Christy et al. [51], who report an abrupt decrease in the symmetric F–H–F stretching frequency, coupled with a splitting of this mode, over the transition. This significant difference in the compression studies further emphasises the dramatic effect that non-hydrostatic conditions may have in altering high-pressure phase behaviour [66–68].

The neutron powder diffraction patterns collected during compression of $NaDF_2$-II (up to a maximum pressure of 4.25 GPa) were successfully refined using the *Pnnm* structural model. A summary of the crystallographic information obtained during compression is shown in Table 5 and Fig. 15. The *c*-axis has been shown to be the most compressible in this form and this can be rationalised in terms of a preferred contraction of the interplanar separation. Compressibility parallel to the *ab*-plane is restricted because the bifluoride ions do not rotate out of this plane – any rotation of the ions remains within the plane.

Upon compression to 4.27 GPa, new peaks appeared in the diffraction pattern that could not be attributed to the orthorhombic form, although the majority of the pattern bore considerable resemblance to those collected for $NaDF_2$-II. Further compression to 4.36 GPa led to these new peaks gaining intensity and at 4.58 GPa a clean diffraction pattern of $NaDF_2$-III was obtained (Fig. 11). The quality of the diffraction pattern collected at this pres-

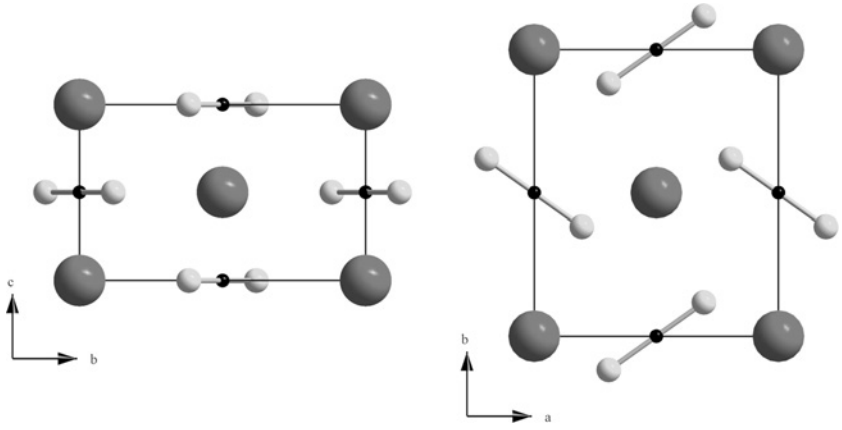

Fig. 14: The orthorhombic structure of $NaDF_2$-II, as determined at 0.66 GPa showing the interlocking of the Na^+ and DF_2^- layers and the rotation of the bifluoride anions within the *ab*-plane.

Tab. 5. Summary of the unit cell data obtained from the Rietveld refinements of the neutron powder diffraction patterns collected for NaDF2-II.

P (GPa)	*a* (Å)	*b* (Å)	*c* (Å)	*V* (Å^3)	V_{mol} (Å^3)	wR_p
0.66	4.7018(13)	5.5147(11)	3.3860(4)	87.796(20)	43.898(20)	0.070
1.11	4.6904(13)	5.4910(10)	3.3647(4)	86.659(20)	43.330(20)	0.070
1.53	4.6810(19)	5.4703(15)	3.3453(6)	85.66(3)	42.83(3)	0.122
2.05	4.6667(12)	5.4511(9)	3.3245(4)	84.572(18)	42.286(18)	0.063
2.62	4.6559(20)	5.4265(15)	3.2995(7)	83.37(3)	41.69(3)	0.160
3.30	4.6432(12)	5.4031(9)	3.2740(4)	82.138(18)	41.069(18)	0.062
3.94	4.6337(18)	5.3817(13)	3.2495(6)	81.03(3)	40.52(3)	0.114
4.25	4.6281(15)	5.3709(11)	3.2390(5)	80.51(2)	40.26(2)	0.080

sure was sufficient to allow indexing to a tetragonal unit cell. In order to confirm the *I*4/*mcm* structure, we performed full-profile Rietveld refinement on this pattern, approximating the initial atomic co-ordinates based on the structure of KHF_2 (see Table 4). The quality of the fit to the diffraction data using this structural model (see Fig. 16) proves conclusively that $NaDF_2$-III does in fact adopt the archetypal structure shared by the larger alkali metal bifluorides and by *y*-NaN_3.

The sluggish nature of the II/III transition suggests that the sample must undergo considerable structural rearrangement at this pressure, evident from a comparison of the structures immediately before and after the transition, see Fig. 17. While a cursory examination of the structures suggests that only a very subtle rotation of half of the anions is required, this belies the wholesale re-organisation of the ions over this transition. For example, the ionic arrangement in form III leads to a much more efficient packing of the sodium cations, as illustrated by the Na…Na polyhedra in Fig. 17. It is interesting to note that this re-arrangement leads to a slight lengthening of bonded Na–F distances, from 2.232(5) Å

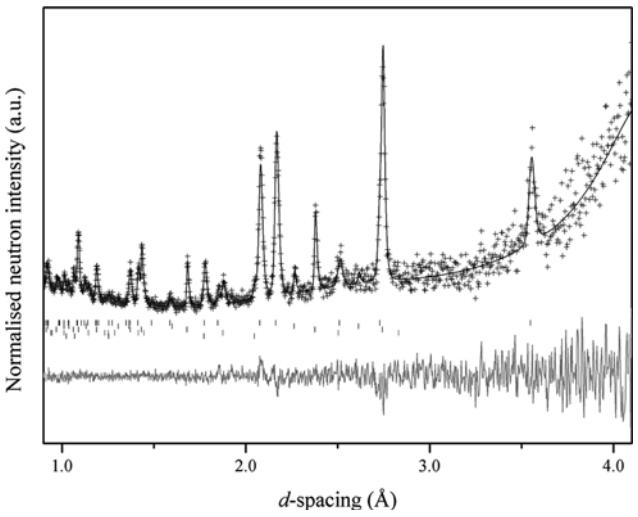

Fig. 16: Rietveld refinement of the pattern collected for $NaDF_2$-III at 7.35 GPa. The experimental data (I_{obs}) are represented as crosses, the calculated pattern (I_{calc}) is shown as a solid line, and the difference ($I_{obs} - I_{calc}$) is shown as the lower line. Tick-marks for each phase ($NaDF_2$-III, Pb, WC, and Ni) are also shown. It has also been necessary to include a small fraction of NaF as an impurity phase (*vide infra*).

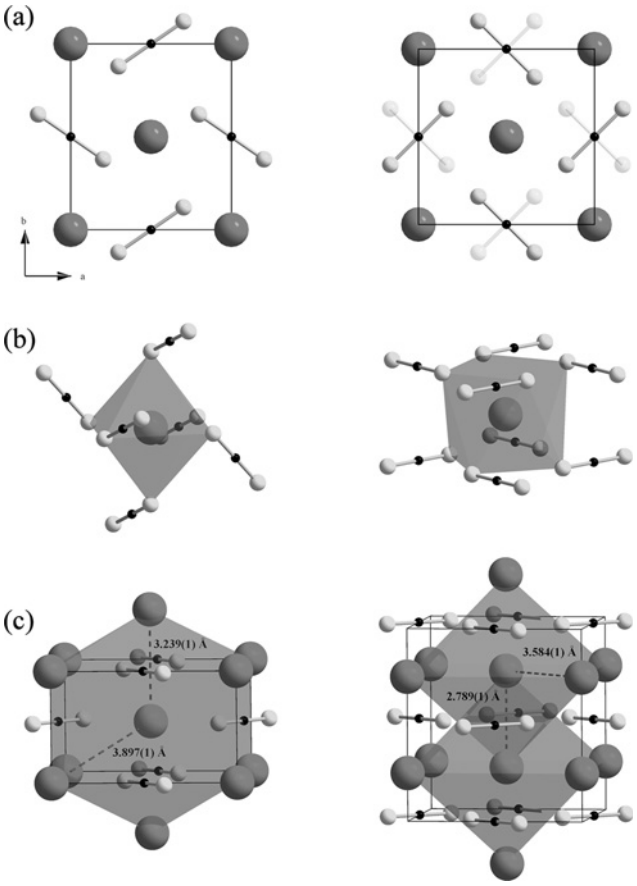

Fig. 17: Comparison of the orthorhombic structure of $NaDF_2$-II (left) with the tetragonal form III (right): (a) the rotation of half of the anions is just part of the considerable structural re-arrangement over this transition; (b) the increase in the sodium co-ordination number shown by Na…F polyhedra; and, (c) the closer packing of sodium cations illustrated by Na…Na polyhedra.

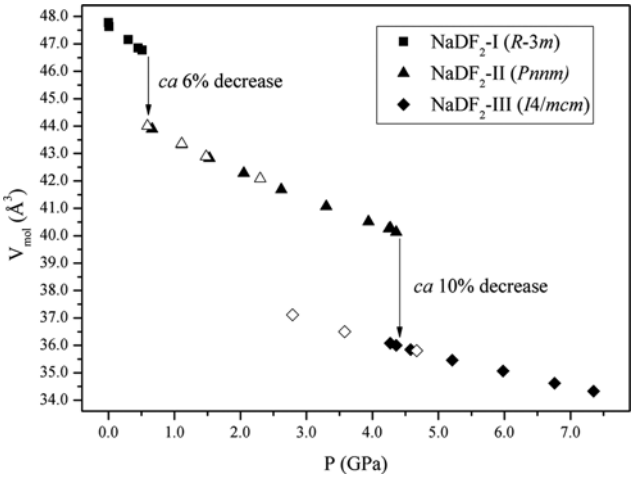

Fig. 18: Plot of the molecular volumes for each of the phases, highlighting the dramatic volume contractions observed over each of the high-pressure phase transitions. Data collected during the decompression are shown as open symbols.

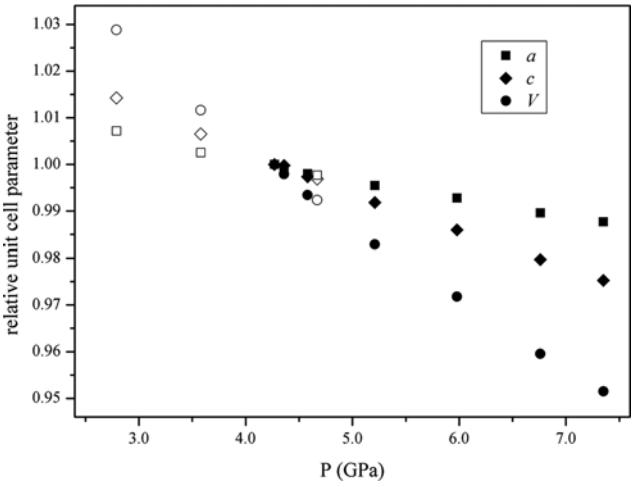

Fig. 19: Relative compression of the unit cell parameters (*a*, *c* and *V*) of $NaDF_2$-III (data have been normalised to the values obtained at 4.27 GPa, the first pressure at which this form was observed during compression).

and 2.251(7) Å in $NaDF_2$-II (4.25 GPa) to 2.362(4) Å at 4.58 GPa. However, this is compensated by the much more favourable anion-anion interactions since the electronegative fluorine atoms of each DF_2^- unit is oriented directly at the electropositive deuterium of its nearest neighbour. The most important aspect of this structural modification, however, is the increase in the co-ordination number of each cation from six in forms I and II to eight in form III. The large reduction in volume (~10%; Fig. 18) also explains the disproportionately large load that was required to increase sample pressure sufficiently to drive the II/III phase transition to completion.

In order to verify the selection of the *I*4/*mcm* structure, we also performed Rietveld refinements using the *P*4/*ncc* structure proposed by Christy et al. [51] using co-ordinates corresponding to the *I*4/*mcm* structure, but with arbitrary displacements applied to unconstrained coordinates. Subsequent refinement of the atomic positions resulted in convergence to the *I*4/*mcm* structure.

A summary of the unit cell parameters obtained by Rietveld refinement of the patterns collected during compression (and decompression) of $NaDF_2$-III is presented in Table 6 and the plot of the relative contraction of the unit cell axes is shown in Fig. 19. As one might expect,

Tab. 6. The unit cell parameters obtained during compression of $NaDF_2$-III, including two datasets for which it was necessary to include both the tetragonal and the orthorhombic phases in the refinement. Data collected during the subsequent decompression are also presented.

P (GPa)	Form	*a* (Å)	*b* (Å)	*c* (Å)	*V* (Å^3)	V_{mol} (Å^3)	wR_p
4.27	II	4.639(4)	5.366(3)	3.2373(11)	80.59(5)	40.30(5)	0.107
	III	5.0793(18)		5.594(3)	144.32(9)	36.08(9)	
4.36	II	4.638(6)	5.361(4)	3.2282(19)	80.27(9)	40.14(9)	0.065
	III	5.0745(8)		5.5928(11)	144.02(4)	36.01(4)	
4.58	III	5.0691(8)		5.5793(11)	143.37(4)	35.84(4)	0.076
5.21	III	5.0563(6)		5.5485(8)	141.85(3)	35.46(3)	0.063
5.98	III	5.0427(8)		5.5154(11)	140.25(4)	35.06(4)	0.072
6.76	III	5.0266(4)		5.4806(7)	138.48(2)	34.62(2)	0.048
7.35	III	5.0169(5)		5.4556(7)	137.32(3)	34.33(3)	0.047
4.67	III	5.0676(11)		5.5767(16)	143.21(6)	35.80(6)	0.167
3.58	III	5.0922(7)		5.6305(10)	146.00(4)	36.50(4)	0.079
2.79	III	5.1156(7)		5.6736(10)	148.48(4)	37.12(4)	0.081
2.30	II	4.669(2)	5.4397(16)	3.3143(7)	84.17(3)	42.09(3)	0.090
1.48	II	4.6809(20)	5.4734(16)	3.3483(7)	85.79(3)	42.90(3)	0.095
1.11	II	4.6926(20)	5.4922(16)	3.3648(6)	86.72(3)	43.36(3)	0.084
0.59	II	4.707(2)	5.5167(20)	3.3894(8)	88.02(4)	44.01(4)	0.117

the *c*-axis, (corresponding to the interplanar separation in the tetragonal structure), is the most compressible. Compression of the *ab*-plane meanwhile manifests itself in the shortening of the F ... D interactions between neighbouring anions – in this pressure range the anions do not rotate and thus the 4-fold rotational symmetry is maintained.

It should be noted that an additional peak was observed in the higher-pressure diffraction patterns ca. 2.2 Å, which has been successfully modelled by the inclusion of a small fraction of NaF (*Fmmm*) [69] as an impurity. It is likely that a small quantity of NaF was formed as a by-product of the synthesis of $NaDF_2$ and, despite its limited solubility in methanol and ethanol, we suggest that dissolution of the small quantities present in the pressure medium meant that this was not observed in the diffraction patterns collected at lower pressures. It was only upon compression to 4.58 GPa that pressure-induced precipitation led to the characteristic NaF diffraction pattern being observed. Therefore high-quality diffraction patterns were collected during the decompression of $NaDF_2$-III in order to discover whether this impurity would disappear below this pressure and this was indeed observed. It is also important to note that the *P*4/*ncc* structure does not adequately model this extraneous peak and we can therefore be confident that this is not a 'superlattice' peak indicative of a unit cell-doubling. A further important feature of this decompression was the significant hysteresis that is observed between forms III and II. The tetragonal form remains stable during decompression to 2.79 GPa, or 1.5 GPa below the transition pressure on compression. This is further evidence of the significant kinetic barrier to this transition, a result of the considerable structural rearrangement that is required. It was only at the next pressure point (2.30 GPa) that a pure sample of phase II was obtained; this phase remained stable during the rest of the decompression study. Unfortunately experimental time constraints meant that it was not possible to obtain diffraction data below 0.59 GPa (i.e. above the I/II transition pressure) and so it is not possible to comment on the recoverability of this phase to atmospheric pressure.

Conclusions

This study of both sodium azide and sodium bifluoride was performed not only to provide invaluable information on the high-pressure behaviour of these materials in isolation, but also to present a comparative study of the effects of non-ambient conditions on compounds that are widely regarded as structural analogues. It is hoped that the structural characterization of these compounds at elevated temperatures and pressures will provide an insight into the compression behaviour of the wider family of compounds with spherical cations and rod-like anions.

Such information is of importance to theoreticians who seek to model the effects of extreme conditions on a range of ionic materials or high-energy processes such as explosive decomposition. Of particular importance is the correlation of the electronic structures of simple azides with their explosive behaviour [1, 3]. The dependence of impact sensitivity on crystal structure has also been explored for selected metal azides [70]. A linear correlation between impact sensitivity and the minimum non-bonded N ... N distance was reported. Although this model is appealing, primarily in its simplicity, the authors admit that no account has been made for thermochemistry, particularly the enthalpies of formation, or for the effects of other stimuli such as heat, static shock or friction. As has been demonstrated in this and previous studies, the effects of extreme conditions on the crystal structures of energetic materials can be dramatic, and often induce phase transitions [71–73]. It is therefore essential to obtain structural information on such materials at a range of temperatures and pressures. For example, the shortest non-bonded N ... N distance in *y*-NaN_3, is ca. 2.8 Å compared to 3.6 Å in the *α*-form (at comparable temperature and pressure). Such a sizeable difference in these values might suggest that the correlation suggested in reference [70] would no longer be valid if the high-pressure, high-temperature *y*-structure were to be considered.

In addition to the dramatic changes in the N ... N intermolecular interactions, the $\alpha \rightarrow y$ transition has been observed to cause an increase in the co-ordination number of sodium from six to eight. In this way, the application of pressure may be regarded as being analogous to moving down a group in the periodic table by forcing the sodium salt to adopt the structures observed for the larger alkali metal azides (KN_3, RbN_3, CsN_3). It would therefore seem reasonable to expect that LiN_3 might also transform under elevated pressures and temperatures to the archetypal CsN_3-II structure. Based on the systematic variations in the transition pressure of the Group 1 chlorides from the NaCl-type structure to CsCl-type structure with cation size [74, 75], one would anticipate higher transition pressure for LiN_3 than for NaN_3.

The co-ordination number of sodium also increases on compression of $NaDF_2$-I and $NaDF_2$-II to give $NaDF_2$-III. The II–III transition is also sluggish, similar to the

$\alpha \rightarrow \gamma$ transition in NaN_3, as a consequence of the significant structural rearrangement. For NaN_3, no evidence was found in the current study for an analogue of the intermediate orthorhombic $NaDF_2$-II, but there is no obvious reason why such a form could not exist. Indeed, it may be that one of the two high-pressure phases identified by Zhu et al. [30] could be a possible candidate.

It worth revisiting Pistorius' suggestion that '*$NaHF_2$-II and NaN_3-III (the y-form) are isostructural... (and) cannot have the tetragonal KN_3 structure*' [31] and Hamann's suggestion that $NaHF_2$-III is unlike KHF_2 [50]. By performing this neutron powder diffraction study we have demonstrated that: (i) $NaDF_2$-II and *y*-NaN_3 are distinct; (ii) *y*-NaN_3 does have the *I*4/*mcm* structure of KN_3; and (iii) $NaDF_2$-III also adopts this structure, a feature it shares with KHF_2. One would therefore suggest that only by performing diffraction studies such as these can high-pressure polymorphism be unequivocally resolved. Moreover, by ensuring that hydrostaticity has been maintained throughout this study we can exclude the possible effects of anisotropic stresses and strains on the high-pressure behaviour of sodium azide and sodium bifluoride. We have attributed the disparity between the results of Christy et al. [51] and those reported herein to the selection of non-hydrostatic conditions employed in the former, stemming from the selection of Nujol as the pressure-transmitting medium. This illustrates the importance of the selection of an appropriate pressure medium based on not only the material under investigation, but also the desired pressure regime. This has particular implications for theoretical studies since only isotropic stress (i.e. hydrostatic pressure) is a thermodynamic variable. It seems unlikely that the differences between the current study and previous compression studies can be attributed to sample deuteration. Although deuteration has been observed to affect the hydrogen bonding within the bifluoride units [41], it is not expected this to alter dramatically the inter-ionic F ... Na interactions. It is the latter interactions that dominate in the crystal packing of all of the forms characterized in this study, as well as in those proposed previously [51]. In fact, it should be underlined that the original motivation for this study of sodium bifluoride was the distinctly unfavourable F ... F interactions that would be observed in the *P*4/*ncc* structure.

Acknowledgements: We thank Dstl and EPSRC for contributions toward a studentship (DIAM), STFC for the provision of neutron beamtime, and MOD WPE for funding under the terms of contract RD028-06366. We are grateful to one of the referees for their very useful feedback on the original manuscript.

References

[1] A. B. Gordienko, Y. N. Zhuravlev, A. S. Poplavnoi, *Phys. Status Solidi B* **1996**, *198*, 707.
[2] É. D. Aluker, Y. N. Zhuravlev, V. Y. Zakharov, N. G. Kravchenko, V. I. Krasheninin, A. S. Poplavnoi, *Russ. Phys. J.* **2003**, *46*, 855.
[3] W. Zhu, J. Xiao, H. Xiao, *J. Phys. Chem. B* **2006**, *110*, 9856.
[4] E. W. Sidebottom, *US Patent Appl.* **1973**, *05/375, 654*.
[5] A. Fuith, *Phase Transitions* **1997**, *62*, 1.
[6] W. Schranz, *Phase Transitions* **1994**, *51*, 1.
[7] S. B. Hendricks, L. Pauling, *J. Am. Chem. Soc.*, **1925**, *47*, 2904.
[8] J. I. Bryant, *J. Chem. Phys.*, **1964**, *40*, 3195.
[9] G. E. Pringle, D. E. Noakes, *Acta Cryst.* **1968**, *B24*, 262.
[10] C. S. Choi, E. Prince, *J. Chem. Phys.* **1976**, *64*, 4510.
[11] E. D. Stevens, H. Hope, *Acta Cryst.* **1977**, *A33*, 723.
[12] S. R. Aghdaee, A. I. M. Rae, *Acta Cryst.* **1984**, *B40*, 214.
[13] Z. Iqbal, *Advances in Raman Spectroscopy* **1972**, *1*, 188.
[14] J. C. Raich, N. S. Gillis, *J. Chem. Phys.* **1976**, *65*, 2088.
[15] J. C. Raich, A. Huller, *J. Chem. Phys.* **1979**, *70*, 3669.
[16] Z. Iqbal, *J. Chem. Phys.* **1973**, *59*, 1769.
[17] R. C. Carling, E. F. Westrum Jnr., *J. Chem. Thermodyn.* **1976**, *8*, 565.
[18] S. Hirotsu, M. Miyamota, K. Ema, *J. Phys. C: Solid State Physics* **1983**, *16*, L661.
[19] M. Midorikawa, H. Orihara, Y. Ishibashi, T. Minato, H. Terauchi, *J. Phys. Soc. Jpn* **1983**, *52*, 3833.
[20] S. Hirotsu, *J. Phys. C: Solid State Physics* **1983**, *16*, L1103.
[21] K. R. Jeffrey, *J. Chem. Phys.* **1977**, *66*, 4677.
[22] S. R. Aghdaee, A. I. M. Rae, *J. Chem. Phys.* **1983**, *79*, 4558.
[23] T. Kushida, R. W. Terhune, *Phys. Rev. B: Condens. Matter* **1986**, *34*, 5791.
[24] G. J. Simonis, C. E. Hathaway, *Phys. Rev. B: Condens. Matter* **1974**, *10*, 4419.
[25] H. J. Müller, J. A. Jöbstl, *Z. Kristallogr.* **1965**, *121*, 385.
[26] R. S. Bradley, J. D. Grace, D. C. Munro, *Z. Kristallogr.* **1964**, *120*, 349.
[27] C. E. Weir, S. Block, G. J. Piermarini, *J. Chem. Phys.* **1970**, *53*, 4265.
[28] C. W. Christoe, Z. Iqbal, *Chem. Phys. Lett.* **1976**, *39*, 511.
[29] K. Knorr, W. Depmeier, *High Pressure Res.* **2000**, *17*, 297.
[30] H. Zhu, F. Zhang, C. Ji, D. Hou, J. Wu, T. Hannon, Y. Ma, *J. Appl. Phys* **2013**, *113*, 033511.
[31] C. W. F. T. Pistorius, A. J. Campbell-White, *High Temperatures – High Pressures* **1970**, *2*, 507.
[32] S. M. Peiris, T. P. Russell, *J. Phys. Chem. A* **2003**, *107*, 944.
[33] M. I. Eremets, M. Y. Popov, I. A. Trojan, V. N. Denisov, R. Boehler, R. J. Hemley, *J. Chem. Phys.* **2004**, *120*, 10618.
[34] H. P. Dixon, H. D. B. Jenkins, T. C. Waddington, *J. Chem. Phys.* **1972**, *57*, 4388.
[35] J. Emsley, *Chem. Soc. Rev.* **1980**, 9, 91.
[36] J. Emsley, R. J. Parker, R. E. Overill, *J. Chem. Soc., Faraday Trans. 2* **1983**, *79*, 1347.
[37] B. L. McGaw, J. A. Ibers, *J. Chem. Phys.* **1963**, *39*, 2677.
[38] J. J. Rush, L. W. Schroeder, A. J. Melveger, *J. Chem. Phys.* **1972** *56*, 2793.

[39] C. J. Ludman, T. C. Waddington, E. K. C. Pang, J. A. S. Smith, *J. Chem. Soc., Faraday Trans. 2* **1977**, *73*, 1003.
[40] R. D. Cooke, C. Pastorek, R. E. Carlson, J. C. Decius, *J. Chem. Phys*. **1978**, *69*, 5.
[41] E. Spinner, *Aust. J. Chem.* **1980**, *33*, 933.
[42] D. Colognesi, A. Pietropaolo, R. Senesi, A. J. Ramirez-Cuesta, *Phys. Rev. B* **2007**, *76*, 174206.
[43] J. M. Williams, L. F. Schneemeyer, *J. Am. Chem. Soc*. **1973**, *95*, 5780.
[44] F. Rinne, H. Hentschel, J. Leonhardt, *Z. Kristallogr*. **1923**, *58*, 629.
[45] C. C. Andersen, O. Hassel, *Z. Phys. Chem.* **1926**, *123*, 151.
[46] R. W. G. Wyckoff, *Crystal Structures*, Interscience, New York, USA, 1954.
[47] S. Troyanov, *Crystallography Reports* **2005**, *50*, 773.
[48] R. Kruh, K. Fuwa, T. E. McEver, *J. Am. Chem. Soc*. **1956**, *78*, 4256.
[49] E. F. Westrum, G. A. Burney, *J. Phys. Chem.* **1961**, *65*, 344.
[50] S. D. Hamann, M. Linton, *Aust. J. Chem.* **1976**, *29*, 479.
[51] A. G. Christy, J. Haines, S. M. Clark, *J. Phys. Condens. Matter* **1992**, *4*, 8131.
[52] R. J. Angel, M. Bujak, J. Zhao, G. D. Gatta, S. D. Jacobsen, *J. Appl. Crystallogr*. **2007**, *40*, 26.
[53] W. G. Marshall, D. J. Francis, *J. Appl. Crystallogr*. **2002**, *35*, 122.
[54] A. D. Fortes, PhD Thesis, University College London, UK **2004**.
[55] J. M. Besson, R. J. Nelmes, G. Hamel, J. S. Loveday, G. Weill, S. Hull, *Physica B* **1992**, *180–181*, 907.
[56] EXPGUI, a graphical user interface for GSAS by B. H. Toby in *J. Appl Cryst*. **2001**, *34*, 210.
[57] W. G. Marshall, D. J. Francis, C. J. Barry, O. Kirichek, C. R. Pulham, M. G. Tucker, *unpublished results*.
[58] F. Birch, *Phys. Rev*. **1947**, *71*, 809.
[59] R. J. Angel, *EOS-FIT V5.2*, Department of Geological Sciences, Virginia Tech., Blacksburg, VA, USA, **2001**.
[60] S. A. Medvedev, I. A. Trojan, M. I. Eremets, T. Palasyuk, T. M. Klapötke, J. Evers, *J. Phys. Condens. Matter* **2009**, *21*, 195404.
[61] H. Spetzler, C. G. Sammis, R. J. O'Connell, *J. Phys. Chem. Solids* **1972**, *33*, 1727.
[62] J. L. Feldman, M. J. Mehl, L. L. Boyer, N. C. Chen, *Phys. Rev. B* **1988**, *37*, 4784.
[63] D. Louër, A. Boultif, *Z. Kristallogr. Suppl.* **2007**, *26*, 191.
[64] U. Müller, *Z. Anorg. Allg. Chem*. **1972**, *392*, 159.
[65] M. J. Buerger, *Am. Mineral.* **1931**, *16*, 361.
[66] J. Haines, J. M. Leger, F. Gorelli, M. Hanfland, *Phys. Rev. Lett.* **2001**, *87*, 155503.
[67] D. Machon, V. P. Dmitriev, P. Bouvier, P. N. Timonin, V. B. Shirokov, H. P. Weber, *Phys. Rev. B* **2003**, *68*, 144104.
[68] R. Resel, M. Oehzelt, K. Shimizu, A. Nakayama, K. Takemura, *Solid State Commun.* **2004**, *129*, 103.
[69] V. Deshpande, *Acta Cryst*. **1961**, *14*, 794.
[70] M. Cartwright, J. Wilkinson, *Propellants, Explos., Pyrotech.* **2010**, **35**, 326.
[71] A. J. Davidson, I. D. H. Oswald, D. J. Francis, A. R. Lennie, W. G. Marshall, D. I. A. Millar, C. R. Pulham, J. E. Warren, A. S. Cumming, *CrystEngComm* **2008**, *10*, 162.
[72] D. I. A. Millar, I. D. H. Oswald, C. Barry, D. J. Francis, W. G. Marshall, C. R. Pulham, A. S. Cumming, *Chem. Commun.* **2010**, *46*, 5662.
[73] D. I. A. Millar, H. E. Maynard-Casely, A. K. Kleppe, W. G. Marshall, C. R. Pulham, A. S. Cumming, *CrystEngComm* **2010**, *12*, 2524.
[74] S. N. Vaidya and G. C. Kennedy, *J. Phys. Chem. Solids* **1971**, *32*, 951.
[75] W. A. Bassett, T. Takahashi, H-K. Mao, S. J. Weaver, *J. Appl. Phys*. **1968**, *39*, 319.

Received May 17, 2013; accepted December 4, 2013
Published online February 13, 2014